PAIN with and without PAR: variants for third-spin assisted heteronuclear polarization transfer

J Biomol NMR (2013) 56:365–377
DOI 10.1007/s10858-013-9756-4

ARTICLE

PAIN with and without PAR: variants for third-spin assisted heteronuclear polarization transfer

Vipin Agarwal · Mariana Sardo · Ingo Scholz · Anja Böckmann · Matthias Ernst · Beat H. Meier

Received: 28 March 2013 / Accepted: 17 June 2013 / Published online: 27 June 2013

Abstract In this article, we describe third-spin assisted heteronuclear recoupling experiments, which play an increasingly important role in measuring long-range heteronuclear couplings, in particular ^{15}N–^{13}C, in proteins. In the proton-assisted insensitive nuclei cross polarization (PAIN-CP) experiment (de Paëpe et al. in J Chem Phys 134:095101, 2011), heteronuclear polarization transfer is always accompanied by homonuclear transfer of the proton-assisted recoupling (PAR) type. We present a phase-alternating experiment that promotes heteronuclear (e.g. $^{15}N \rightarrow {}^{13}C$) polarization transfer while simultaneously minimizing homonuclear (e.g.$^{13}C \rightarrow {}^{13}C$) transfer (PAIN without PAR). This minimization of homonuclear polarization transfer is based on the principle of the resonant second-order transfer (RESORT) recoupling scheme where the passive proton spins are irradiated by a phase-alternating sequence and the modulation frequency is matched to an integer multiple of the spinning frequency. The similarities and differences between the PAIN-CP and this het-RESORT experiment are discussed here.

Keywords Solid-state NMR · Heteronuclear correlation · PAIN-CP · RESORT · Heteronuclear RESORT

Introduction

Polarization transfer between spins is one of the most fundamental building blocks in NMR experiments in material sciences, chemistry, and biology (Cavanagh et al. 2007; Ernst 1989). In multi-dimensional solid-state NMR, dipolar-coupling based cross-peaks are key for the assignment of resonances and the determination of distances and torsion angles that are needed to determine protein structures (Castellani et al. 2002; Loquet et al. 2008; Manolikas et al. 2008; van Melckebeke et al. 2010; Wasmer et al. 2008; Zech et al. 2005; Zhou et al. 2007). However, dipolar couplings are averaged out under magic-angle spinning (MAS), and they have to be selectively reintroduced during polarization-transfer steps by means of dipolar-recoupling schemes (Bennett et al. 1994, 1998; Brinkmann et al. 2000; de Paepe et al. 2006, 2012; Hohwy et al. 1998; Meier and Earl 1987; Nielsen et al. 2012; Tycko and Dabbagh 1990; Verel et al. 1997, 2001). Most recoupling techniques generate a zero-quantum (ZQ) or a double-quantum (DQ) Hamiltonian in the first-order effective Hamiltonian, and are subject to dipolar truncation (Bayro et al. 2009; Hohwy et al. 1999, 2002). The term "dipolar truncation" relates to the phenomenon that polarization transfer across weak couplings is strongly attenuated in the presence of strong couplings. Dipolar

Vipin Agarval and Mariana Sardo equally contributed to this work.

Electronic supplementary material The online version of this article (doi:10.1007/s10858-013-9756-4) contains supplementary material, which is available to authorized users.

V. Agarwal · M. Sardo · I. Scholz · M. Ernst (✉) · B. H. Meier (✉)
Physical Chemistry, ETH Zurich, 8093 Zurich, Switzerland
e-mail: maer@ethz.ch

B. H. Meier
e-mail: beme@ethz.ch

M. Sardo
Chemistry Department, CICECO, University of Aveiro, 3810-193 Aveiro, Portugal

A. Böckmann (✉)
IBCP, UMR 5086 CNRS, Université de Lyon 1, 7 Passage du Vercors, 69367 Lyon, France
e-mail: a.bockmann@ibcp.fr

truncation implies that such recoupling sequences cannot be used to sensitively measure long distances in uniformly labeled samples if a pair of nuclei of the same type with a shorter distance is present. While either measuring samples with specifically labeled spin-pairs (Castellani et al. 2002; Hong and Jakes 1999; LeMaster and Kushlan 1996; Loquet et al. 2011; Zech et al. 2005) or frequency selective recoupling methods (Jaroniec et al. 2001; Verhoeven et al. 2004; Williamson et al. 2003) can alleviate the consequences of dipolar truncation, there are many benefits of working with uniformly [^{13}C, ^{15}N] labeled samples using non-selective recoupling methods.

Second-order recoupling sequences provide a spectroscopic method to significantly reduce the problem of dipolar truncation and allow the determination of long-range distance restraints in uniformly labeled biomolecules. Such sequences are based on cross terms between homonuclear or heteronuclear dipolar couplings to a "third spin", often a proton, in the second-order effective Hamiltonian. Several second-order recoupling sequences have been reported in the literature e.g. proton-driven spin diffusion (PDSD) (Grommek et al. 2006; Kubo and McDowell 1988; Suter and Ernst 1985; Szeverenyi et al. 1982), dipolar-assisted recoupling (DARR) (Takegoshi et al. 2001, 2003; Morcombe et al. 2004, the CHHC/NHHC experiments (Heise et al. 2005; Lange et al. 2002, 2003; Loquet et al. 2008), proton-assisted recoupling (PAR) (de Paepe et al. 2008), proton-assisted insensitive nuclei cross polarization (PAIN-CP) (de Paepe et al. 2011; Lewandowski et al. 2007), mixed-rotational and rotary-resonance recoupling (MIRROR) (Scholz et al. 2008) and resonant second-order transfer (RESORT) (Scholz et al. 2010a). Some of the second-order sequences have been shown to work at fast MAS frequencies despite the fact that the magnitude of the cross terms decrease with increasing MAS frequency (Lewandowski et al. 2009; Scholz 2010; Scholz et al. 2008).

The PAR and PAIN-CP experiments are second-order recoupling sequences that lead to polarization transfer between two S spin nuclei (PAR) or an S-M spin pair (PAIN-CP). The transfer is based on the cross terms between the two I–S heteronuclear dipolar couplings (PAR) or the I–S and I–M heteronuclear dipolar couplings (PAIN-CP). Here, the "third spin" is denoted by I, which is usually a proton that is coupled to the two spins between which polarization transfer is observed. Technically speaking, the PAR experiment is a homonuclear non-resonant ZQ experiment, while the PAIN-CP experiment is a heteronuclear resonant experiment that promotes ZQ or DQ polarization transfer.

The heteronuclear polarization transfer in PAIN-CP is always accompanied by homonuclear PAR transfer, and it is experimentally impossible to separate PAIN-CP from PAR by optimizing the experimental rf amplitudes (vide infra). Hence, in a 2D PAIN-CP spectrum, ^{15}N–^{13}C heteronuclear polarization transfer is always accompanied by ^{13}C–^{13}C homonuclear transfer, resulting in ^{15}N–(^{13}C)–^{13}C peaks in the PAIN-CP spectrum. The simultaneous occurrence of the two polarization-transfer conditions has been exploited to simultaneously record PAIN and PAR spectra in a single two-dimensional experiment without compromising the signal-to-noise (Lamley and Lewandowski 2012; Nielsen et al. 2012). In other situations, it is beneficial to suppress the ^{13}C homonuclear transfer to only detect direct ^{15}N–^{13}C correlations. This is of particular interest in ^{13}C/^{15}N mixed samples that are used to characterize interfaces, for example between monomers in multimers or polymers, between proteins and their ligands, or between different domains (de Paepe et al. 2011; Etzkorn et al. 2004; Helmus et al. 2011; Marulanda et al. 2004; Seuring et al. 2012; van Melckebeke et al. 2010).

In this contribution we propose a new heteronuclear second-order recoupling sequence based on the principles of RESORT (Scholz, 2010). The sequence, dubbed as heteronuclear-RESORT (het-RESORT), promotes heteronuclear polarization transfer while at the same time suppressing homonuclear polarization transfer. We envisage the main application of the sequence would be to attenuate homonuclear transfer while still observing heteronuclear contacts arising from third spin assisted recoupling. The advantage of such a scheme is that the heteronuclear polarization transfer will not be distributed over many different cross peaks through the homonuclear relay transfer. Furthermore, longer distances can be directly measured if the relayed transfer is greatly attenuated. An important practical application is the measurement of intermolecular distances in mixed-labeled samples (de Paepe et al. 2011; van Melckebeke et al. 2010). However for sensitivity reasons, this methodological study is performed on uniformly labeled protein. The het-RESORT is based on the resonant second-order cross terms between the N–H and C–H dipolar couplings. First we qualitatively explain the principles of het-RESORT and compare it to PAIN-CP recoupling. Further, through simulation and experiments, we demonstrate that the RESORT condition can be used to separate the homonuclear and heteronuclear transfer by appropriate setting of the experimental parameters. 1,2-^{13}C-glycine ethylester is used as a model system to characterize the main features of the het-RESORT recoupling scheme. As an application of the method, the attenuation of the competitive homonuclear polarization transfer, while maintaining the heteronuclear transfer, is demonstrated on U-[^{13}C,^{15}N]-ubiquitin.

Qualitative description of the het-RESORT experiment

A description of the PAIN-CP experiment (Fig. 1a) has to take into account the four frequencies that modulate the interaction-frame Hamiltonian: the MAS frequency ω_r and

the three nutation frequencies ω_{1I}, ω_{1S}, and ω_{1M} (typically, I = ^{1}H, S = ^{13}C, M = ^{15}N) corresponding to the rf-field amplitudes of the three spin-lock fields. Such a time-dependent Hamiltonian can be analyzed in the framework of operator-based Floquet theory (Leskes et al. 2010; Scholz et al. 2010b) to obtain effective Hamiltonians. The PAIN-CP experiment can be performed at resonance conditions given by $n_0\omega_r \mp \omega_{1S} \pm \omega_{1M} = 0$ where $n_0 = 0$, ±1, ±2, ±3, ±4. Since PAIN-CP is a second-order recoupling condition, we need to discuss the second-order effective Hamiltonian

$$\bar{\mathscr{H}}^{(2)} = \mathscr{H}^{(0,0,0,0)}_{(2)} + \mathscr{H}^{(n_0,+1,-1,0)}_{(2)} + \mathscr{H}^{(-n_0,-1,+1,0)}_{(2)} \quad (1)$$

where $\mathscr{H}^{(n_0,+1,\mp1,0)}_{(2)}$ and $\mathscr{H}^{(0,0,0,0)}_{(2)}$ represent the resonant and the non-resonant parts of the effective Hamiltonian. The resonant second-order PAIN-CP Hamiltonian has the form

$$\mathscr{H}^{(\pm n_0,\pm1,\mp1,0)}_{(2)} = \sum_{p,q,r} c_{IMS}(p,q,r) 2I_{pz}M_q^{\mp}S_r^{\pm} + \sum_{\substack{p,q,r \\ p<r}} c_{MS}(p,q,r) 2S_{pz}M_q^{\mp}S_r^{\pm} \quad (2)$$

The three spin terms $I_{pz}M_q^{\mp}S_r^{\pm}$ are responsible for promoting second-order heteronuclear polarization transfer between the S and M spins and results from the cross-term between M–I and S–I dipolar couplings.

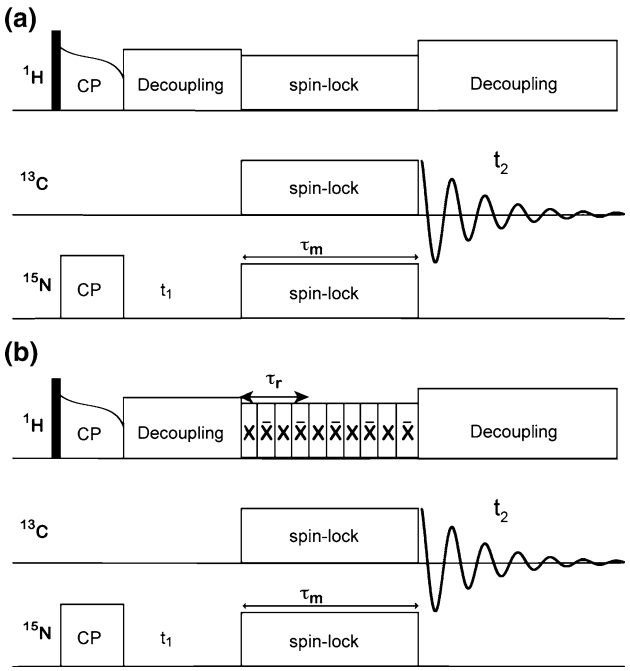

Fig. 1 Pulse sequence for 2D ^{15}N(M)–^{13}C(S) chemical-shift correlation experiment with **a** PAIN and **b** het-RESORT mixing. The timing for the n = 2 het-RESORT condition is indicated in the figure. In case of the PAIN-CP experiment the phase-alternating pulses on the I (^{1}H) spins is replaced with a cw spinlock pulse

Note that, in addition, first-order heteronuclear polarization transfer can occur at the $n_0\omega_r \mp \omega_{1S} \pm \omega_{1M} = 0$ resonance condition (Hartmann–Hahn CP) when $n_0 = \pm2$, ±1. These conditions have to be avoided for PAIN-CP experiment, which is usually performed at the $n_0 = 0$ condition, where the first-order contribution to the direct M → S CP transfer is zero. However, it is worth noting that for all values of n_0, in particular also for $n_0 = 0$, there are second-order CP conditions (Lange et al. 2009) with contributions from cross terms between homonuclear (S–S) and heteronuclear (M–S) dipolar couplings. The contribution of the second-order CP terms, especially at longer mixing times (10–20 ms), is on the order of one-bond nitrogen carbon scalar couplings for directly bonded S–M spin pairs.

The non-resonant second-order contribution to the effective Hamiltonian has the form

$$\begin{aligned}\mathscr{H}^{(0,0,0,0)}_{(2)} = &\sum_{p,q,r} c_{IMM}(p,q,r) 2I_{pz}M_q^{\pm}M_r^{\mp} \\ &+ \sum_{p,q,r} c_{ISS}(p,q,r) 2I_{pz}S_q^{\pm}S_r^{\mp} \\ &+ \sum_{p} c_M(p) 2M_{pz} + \sum_{p} c_S(p) 2S_{pz} \\ &+ \sum_{p} c_I(p) 2I_{pz}\end{aligned} \quad (3)$$

which is completely equivalent to the terms appearing in the homonuclear PAR experiment (de Paepe et al. 2008; Scholz et al. 2007). The presence of three-spin terms ($I_{pz}S_q^{\pm}S_r^{\mp}$ and $I_{pz}M_q^{\pm}M_r^{\mp}$), promote homonuclear S- and M-spin polarization transfer responsible for the PAR transfer during the PAIN-CP experiment. Individually, both the PAR and PAIN-CP terms are large for all rf-field amplitudes. However, the efficiency and details of both the homonuclear and heteronuclear polarization transfer is determined by the one-spin fictitious-field operators S_{pz} and M_{pz} in the non-resonant second-order Hamiltonian. As discussed previously (de Paepe et al. 2008, 2011; Scholz et al. 2007), these terms can truncate the transfer terms, and both the homonuclear and heteronuclear polarization transfers are only efficient in the regions where the contribution of the one-spin operators S_{pz} and M_{pz} is small compared to the three-spin ZQ operators. There is no obvious way to separate PAR and PAIN transfer pathways, since conditions for good transfer are selected by minimizing the same one-spin terms in the non-resonant part of the effective Hamiltonian.

In the het-RESORT experiment (Fig. 1b), the continuous wave (CW) irradiation on the protons is replaced by a phase-alternating irradiation with a modulation frequency ω_m while the two active spins are still irradiated with CW rf fields corresponding to nutation frequencies ω_{1S} and ω_{1M}. The Hamiltonian is again modulated with four frequencies,

ω_r, ω_{1S}, ω_{1M}, and ω_m which need to be included in the Floquet description. In general, the second-order heteronuclear transfer is achieved when the four modulation frequencies satisfy the general resonance condition $n_0\omega_r + k_0\omega_{1S} \pm h_0\omega_{1M} + \ell_0\omega_m = 0$. Here, n_0, k_0, h_0, ℓ_0 are the four Fourier numbers corresponding to the four frequencies, and can have the following values in order to achieve second-order recoupling: $\ell_0 = -\infty$ to $+\infty$, $k_0, h_0 = 0, \pm1, \pm2$ and $n_0 = 0, \pm1, \pm2, \pm3, \pm4$. The different combinations of the four Fourier numbers can generate a large number of resonance conditions where a PAIN-CP-like second-order heteronuclear polarization transfer similar to the RESORT experiment can be achieved, and careful adjustment of the experimental conditions is necessary to choose the desired effective Hamiltonian.

In particular, the combination of the Fourier numbers $n_0 = 1, k_0 = \pm1, h_0 = \mp1, \ell_0 = -1$ generates a resonance condition $\omega_r \pm \omega_{1S} \mp \omega_{1M} - \omega_m = 0$. The second-order effective Hamiltonian at this resonance condition is given by

$$\mathscr{H}_{(2)}^{(1,\pm1,\mp1,-1)} = \sum_{p,q,r} c_{IMS}(p,q,r) 2I_{pz}M_q^{\mp}S_r^{\pm} \tag{4}$$

and contains the heteronuclear three-spin terms that give the desired second-order heteronuclear polarization transfer, while the second-order non-resonant effective Hamiltonian has the general form:

$$\mathscr{H}_{(2)}^{(0,0,0,0)} = \sum_p c_M(p) 2M_{pz} + \sum_p c_S(p) 2S_{pz} + \sum_p c_I(p) 2I_{pz} \tag{5}$$

The $\mathscr{H}_{(2)}^{(0,0,0,0)}$ term contains only one-spin fictitious-field terms, as the potential three-spin terms that appear in the non-resonant terms of the PAIN experiment are zero due to symmetry considerations for the Fourier coefficients of the interaction-frame transformation (Ernst et al. 2006; Scholz et al. 2010b). Again, the one-spin terms in the non-resonant part of the Hamiltonian are responsible for determining the experimental details of rf amplitudes and polarization-transfer efficiencies. This appears to be an ideal scenario to produce a pulse sequence that promotes only heteronuclear transfer, as we have eliminated the homonuclear (in terms of S and M spins) three spin terms ($I_{pz}S_q^{\pm}S_r^{\mp}$) from the non-resonant second-order Hamiltonian, while at the same time selecting only the heteronuclear three spin terms from the resonant second-order Hamiltonian. This condition promotes PAIN-like transfer without simultaneous PAR transfer.

However, on closer examination of the $\omega_r \pm \omega_{13C} \mp \omega_{15N} - \omega_m = 0$ resonance condition, it is apparent that depending upon the chosen parameters two more resonance conditions can be independently and simultaneously satisfied: the two-frequency resonance condition described by $n_0\omega_r + \ell_0\omega_m = 0$, and the three-frequency resonance condition defined by $n_0\omega_r \pm \omega_{1M} \mp \omega_{1S} = 0$. Similar to the PAIN-CP experiment, the three-frequency matching condition represents the Hartmann-Hahn CP condition and can contribute to both first and second-order effective Hamiltonians. The first-order contribution becomes significant only if $\omega_{1I} \gg 3\omega_{1S}, 3\omega_{1M}$ or when the spin-lock rf amplitudes on the S and M spins are sufficiently high that no decoupling is required on the I spins. But even in the regime when $\omega_{1I} \sim \omega_{1S}, \omega_{1M}$, there will always be some amount of direct M $\rightarrow$ S transfer. Again, like in the PAIN-CP there will be a small second-order Hartmann-Hahn CP contribution. The first- and second-order effective Hamiltonians for the conditions are given by:

$$\begin{aligned} \mathscr{H}_{(1)}^{(1,\pm1,\mp1,0)} &= \sum_{q,r} c_{MS}(q,r) 2M_q^{\mp}S_r^{\pm} \\ \mathscr{H}_{(2)}^{(1,\pm1,\mp1,0)} &= \sum_{\substack{p,q,r \\ p<r}} c_{MS}(p,q,r) 2S_{pz}M_q^{\mp}S_r^{\pm} \end{aligned} \tag{6}$$

The two-frequency resonance condition $n_0\omega_r + \ell_0\omega_m = 0$ is the general condition for the homonuclear RESORT experiment (Scholz et al. 2010a). The second-order effective Hamiltonian at the two-frequency resonant condition is given by:

$$\begin{aligned} \mathscr{H}_{(2)}^{(n_0,0,0,\ell_0)} = &\sum_{p,q,r} c_{IMM}(p,q,r) 2I_{pz}M_q^{\pm}M_r^{\mp} \\ &+ \sum_{p,q,r} c_{ISS}(p,q,r) 2I_{pz}S_q^{\pm}S_r^{\mp} + \sum_p c_M(p) 2M_{pz} \\ &+ \sum_p c_S(p) 2S_{pz} \end{aligned} \tag{7}$$

and contains homonuclear RESORT-type three-spin terms. When optimizing the het-RESORT experiment, we have to choose the rf-field amplitudes and modulation frequencies such that (1) the contribution by the $\mathscr{H}_{(2)}^{(n_0,0,0,\ell_0)}$ term is minimized (homonuclear transfer), (2) the contribution by the $\mathscr{H}_{(2)}^{(n_0,\pm1,\pm1,\ell_0)}$ terms (heteronuclear transfer) is maximized and (3) the one-spin terms in $\mathscr{H}_{(2)}^{(0,0,0,0)}$ are minimized. To summarize, the complete effective Hamiltonian at the $\omega_r \pm \omega_{1S} \mp \omega_{1M} + \omega_m = 0$ resonance condition is given by:

$$\begin{aligned} \bar{\mathscr{H}}^{(2)} = &\mathscr{H}_{(1)}^{(\pm n_0,\pm1,\mp1,0)} + \mathscr{H}_{(2)}^{(0,0,0,0)} + \mathscr{H}_{(2)}^{(\pm n_0,0,0,\mp\ell_0)} \\ &+ \mathscr{H}_{(2)}^{(\pm n_0,\pm1,\mp1,0)} + \mathscr{H}_{(2)}^{(\pm n_0,\pm1,\mp,\mp\ell_0)} \end{aligned} \tag{8}$$

We have investigated this resonance condition in detail through simulations and experiments and present our results below.

There are a large number of further resonance conditions such as $\omega_{1S} \mp \omega_{1M} \pm \ell_0\omega_m = 0$, $\pm 4\omega_r \pm \omega_{1S} \mp \omega_{1M} \mp 5\omega_m = 0$ or even $\omega_r \pm \omega_{1S} \mp \omega_{1M} + \omega_m = 0$ at specific rf amplitudes that selectively promote only second-order heteronuclear transfer. The main differences between all these conditions are: (1) the scaling factor in front of the different spin operators and (2) the number of different sub-resonance conditions. Here we concentrate on the $\omega_r \pm \omega_{1S} \mp \omega_{1M} + \omega_m = 0$ resonance condition. A detailed analysis, comprising a full description and comparison of all possible resonance conditions is complex and will be the subject of future studies.

Numerical simulations

To explore the parameter space of both the PAIN-CP as well as the het-RESORT experiments, numerical simulations were performed using the GAMMA spin-simulation environment (Smith et al., 1994). The results support the difference in the properties of the PAIN-CP/PAR and the het-RESORT/RESORT resonance condition as discussed above. Figure 2 shows a plot of the polarization-transfer efficiency as a function of selected parameters for the heteronuclear as well as homonuclear transfer pathways for the two experiments. Simulations were performed for I = ^{1}H, S = ^{13}C and M = ^{15}N. At a chosen spinning frequency, the PAIN-CP experiment has three independent parameters (ω_{1H}, ω_{13C}, ω_{15N}) that can be optimized, while the PAR experiment has only two independent parameters (ω_{1H}, ω_{13C}). From the theory shown above, the resonance conditions for the PAIN experiment are given by $\omega_{13C} \pm \omega_{15N} = n\omega_r$. From the work of Griffin and coworkers (de Paepe et al. 2008, 2011) we know that the best condition to perform PAIN-CP is at $\omega_{13C} = \omega_{15N}$. Hence, in the present context, only a two-parameter (ω_{1H}, $\omega_{13C} = \omega_{15N}$) simulation is required for optimization of the PAIN-CP and PAR condition. Figure 2a, b show the dependence of the PAIN-CP and PAR transfer on the ^{1}H and ^{15}N (equal to ^{13}C) nutation frequencies. As predicted by the Floquet description, the plot shows that the PAIN-CP and PAR recoupling schemes have an identical dependence on these two experimental parameters and will, therefore, always appear simultaneously. This confirms that the heteronuclear PAIN transfer is always accompanied by a homonuclear PAR transfer. These simulations were performed on a four spin system of the type: $N^{(1)}$–H $\leftrightarrow$ H–$C^{(2)}$ and $C^{(1)}$–H $\leftrightarrow$ H–$C^{(2)}$ where the dashes indicate directly bonded nuclei and the arrows through-space contacts. The detailed spin-system parameters are listed in the Supplementary Information.

In the case of het-RESORT, again at a given MAS frequency, four independent parameters (ω_{1H}, ω_{13C}, ω_{15N}, ω_m) need to be optimized, while the RESORT condition depends only upon three independent parameters (ω_{1H}, ω_{13C}, ω_m). In principle, a four dimensional simulation needs to be performed in order to find the optimum experimental het-RESORT condition. To explore the influence of these parameters, two frequencies were held constant while the other two were varied in order to find all possible resonance conditions. Ideal three-spin systems of the type $N^{(1)}$–H $\leftrightarrow$ $C^{(2)}$ and $C^{(1)}$–H $\leftrightarrow$ $C^{(2)}$ were considered during simulation of the two experiments. At constant ^{1}H (67 kHz) and ^{15}N (50 kHz) nutation frequencies, the polarization transfer was simulated as a function of the modulation frequency ω_m and the ^{13}C nutation frequency ω_{13C}. Figure 2c shows, as expected, a large number of resonance conditions at which het-RESORT polarization transfer is possible. All the resonance conditions are explained by varying the allowed Fourier number in the general resonance condition $n_0\omega_r + k_0\omega_{13C} \pm h_0\omega_{15N} + \ell_0\omega_m = 0$. For ZQ transfer (represented by positive contours and superimposed red lines in Fig. 2c) the signs of k_0 and ℓ_0 have to be opposite, while for DQ transfer (represented by negative contours and superimposed black lines) the signs of k_0 and ℓ_0 have to be the same. In principle, the het-RESORT recoupling experiment can be performed at any of these recoupling conditions, bearing in mind that the corresponding RESORT transfer should be minimized.

From the large set of resonance conditions available, we choose to investigate the one corresponding to $\omega_r + \omega_{13C} - \omega_{15N} + \omega_m = 0$. From the properties of the RESORT experiment we know that the RESORT transfer is poor when the nutation frequency of the heteronuclear spins is larger than 80 kHz (Scholz et al. 2010a). Therefore, the rf field on ^{13}C was set to 90 kHz while the ^{15}N amplitude was kept at 50 kHz. These conditions leave us with only two parameters (ω_{1H}, ω_m) that need to be optimized. The resulting heteronuclear polarization-transfer dependence is shown in Fig. 2d. The corresponding homonuclear RESORT polarization-transfer dependence is shown in Fig. 2e. From the comparison of the two simulations it is apparent that there are many regions where both hetero and homonuclear polarization transfer are equally efficient. However, there exist at least two conditions (indicated by black dotted boxes) where the heteronuclear transfer is good while the homonuclear transfer is weak. Figure 2d shows that the resonance condition in the ω_m dimension are very narrow (in fact a narrow as the $\omega_{15N} = \omega_{13C}$ condition in PAIN) and should be set accurately in order to get heteronuclear polarization transfer. As this is a modulation frequency, it can be set accurately and no experimental optimization of ω_m is required. The complexities of setting up experimental parameters on ^{13}C and ^{15}N channels remain identical in the PAIN and the het-RESORT experiment.

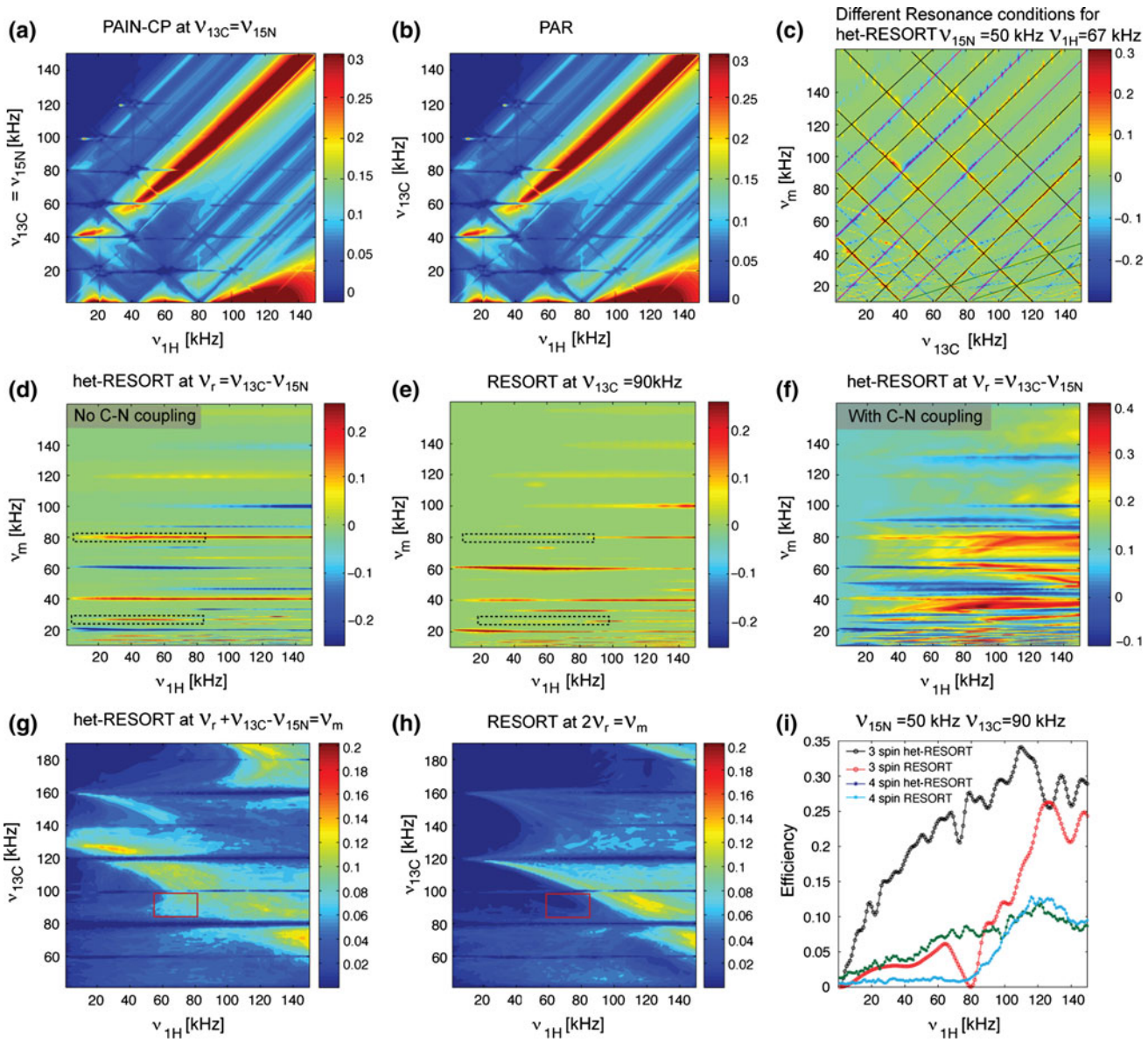

Fig. 2 Numerical simulation of the polarization-transfer efficiencies for heteronuclear and homonuclear PAIN-CP/PAR recoupling schemes in comparison to the het-RESORT and RESORT recoupling scheme. All simulations were performed in GAMMA simulation environment using a three or a four spin system of the types: (1) $N^{(1)}$–$H \leftrightarrow C^{(2)}$ and $C^{(1)}$–$H \leftrightarrow C^{(2)}$ or (2) $N^{(1)}$–$H \leftrightarrow H$–$C^{(2)}$ and $C^{(1)}$–$H \leftrightarrow H$–$C^{(2)}$ spin systems for heteronuclear and homonuclear transfer respectively, where $^{(1)}$ and $^{(2)}$ represent spin numbers. Simulation **a**, **b**, **g** and **h** were performed with a spin-system having four spins while **c**–**f** were performed with spin-system having only three spins. All dipolar couplings were included except the N–C dipolar coupling in the heteronuclear and the C–C dipolar couplings in case of the homonuclear transfer simulation. The isotropic chemical shifts and scalar couplings were set to zero. All spins are irradiated on resonance. The MAS frequency was set to 40 kHz and the ^{1}H and ^{15}N rf fields were varied from 1 to 150 kHz in steps of 1 kHz. The mixing time was set to 4 ms in all the simulations. 144 crystal orientations were considered for powder averaging. The initial magnetization was on spin (1). Intensity optimization plot for **a** PAIN-CP and **b** residual PAR at commonly used experimental condition of $\nu_{13C} = \nu_{15N}$. **c** Simulation of different possible resonance condition for het-RESORT recoupling sequence at $\nu_{15N} = 50$ kHz while $\nu_{1H} = 67$ kHz. A very large number of resonance conditions are observed. **d** Optimization of ν_{xix} versus ν_{1H} for het-RESORT at the resonance condition $\omega_r = \omega_{13C} - \omega_{15N}$. The ν_{15N} and ν_{13C} nutation frequencies were set to 50 and 90 kHz respectively. **e** The dependence of residual homonuclear RESORT transfer as a function of ν_{xix} versus ν_{1H} at $\nu_{13C} = 90$ kHz. **f** Simulation at exactly identical condition as simulation in **d** except that direct N–C couplings were included. Intensity optimization for het-RESORT **g** at the resonance condition $\omega_r = \omega_m - \omega_{15N} + \omega_{13C}$ (and sub-resonance conditions $\omega_m = 2\omega_r$, $\omega_r = \omega_{13C} - \omega_{15N}$). **h** RESORT at the resonance condition $\omega_m = 2\omega_r$. **i** Slice out of the 2D optimization in **g** and **h** at $\nu_{15N} = 50$ kHz for a four-spin system. For comparison identical simulation for a three spin system NHC and CHC is shown

The simulations of Fig. 2d, e were performed with direct N–C dipolar and scalar couplings set to zero. Including the direct N–C coupling into the simulations (Fig. 2f) results in substantial changes in the heteronuclear polarization-transfer profile. The simulation shows an increase in efficiency and broadening of the N → C transfer condition. As discussed above, these additional contributions arise from simultaneous N → C cross-polarization type transfers occurring simultaneously with the desired third-spin mediated transfer.

Figure 2g, h show a simulation of heteronuclear and homonuclear RESORT transfer as a function of ^{1}H and ^{13}C nutation frequencies at a selected resonance condition, $\omega_r = \omega_m - \omega_{15N} + \omega_{13C}$, which simultaneously satisfies the sub-resonance conditions $\omega_m = 2\omega_r$, $\omega_r = \omega_{13C} - \omega_{15N}$. This is the condition we used experimentally. From a comparison of the two polarization-transfer plots it is clearly visible that RESORT and het-RESORT show different dependencies on the experimental parameters. The red boxes in Fig. 2g, h denote the realistically available experimental conditions where substantial heteronuclear transfer is possible while simultaneously attenuating homonuclear transfer. An overlay of slices from Fig. 2g and h at $\nu_{15N} = 50$ kHz is shown in Fig. 2i. The het-RESORT (black) and RESORT (red) transfer curves for an ideal three-spin system (NHC & CHC) show that at $\nu_{1H} = 80$ kHz the homonuclear transfer is completely suppressed. An identical simulation (green and blue) for a more realistic four spin-system shows that the homonuclear transfer is not zero but attenuated five to eightfolds in comparison to the heteronuclear transfer for ^{1}H amplitude between 55 and 80 kHz. So, by simply adjusting the ^{1}H amplitude one can tune the efficiency and the ratio of the heteronuclear to homonuclear polarization transfer. The exact degree of attenuation of homonuclear transfer and details of the intensity optimization curves will vary from the ideal simulation depending on the geometry of the spin system, chemical-shift anisotropy and offsets.

Materials and methods

Uniformly [^{13}C, ^{15}N] labeled microcrystalline ubiquitin was prepared as described previously (Schubert et al., 2006). The experiments at 40 kHz MAS were carried out on a 14.1 T (corresponding ^{1}H-resonance frequency 600 MHz) NMR spectrometer (Bruker Biospin, Germany) equipped with a home-built 1.8 mm triple resonance probe (Samoson et al. 2001). All experiments were performed at cooling gas temperatures of 298 K (U-[^{13}C, ^{15}N] glycine ethylester), and 235 K (Ubiquitin) resulting in a sample temperature of about 12 °C, as determined from the water resonance (Böckmann et al. 2009). Rotors were filled using an ultracentrifugation tool (Böckmann et al. 2009). Experiment-specific details are provided in the corresponding figure captions and in the Supporting Information. All spectra recorded on Ubiquitin were processed in TopSpin 2.0 (Bruker Biospin) by zero filling to no more than double the number of points measured and apodized in both dimensions using a 2.2 shifted squared sine-bell function. The spectra were analyzed and plotted by using CCPNmr Analysis (Stevens et al. 2011; Vranken et al. 2005).

Experimental results and discussion

Based on the theoretical calculations and the numerical simulations, we experimentally investigated a particular resonance condition in more detail. The selected resonance condition is characterized by $\omega_m - \omega_r + \omega_{13C} - \omega_{15N} = 0$ leading to satisfaction of the $\omega_m = 2\omega_r$ and $\omega_r = \omega_{13C} - \omega_{15N}$ resonance conditions. Under these conditions, setting the spinning frequency to 40 kHz directly fixes the modulation frequency to 80 kHz ($\tau_p = 6.25$ µs) and the difference between the ω_{13C} and ω_{15N} rf fields. Hence, only two experimental parameters need to be optimized: the proton rf-field amplitude ω_{1H} and either the ω_{13C} or ω_{15N} rf-field amplitude, while independently crosschecking that the corresponding homonuclear transfer is minimized for those values.

Figure 3 shows the experimental polarization-transfer efficiencies for the RESORT/het-RESORT and PAR/PAIN-CP experiments as a function of the mixing time (τ_{mix}) and the proton rf-field amplitude ν_{1H} at a MAS frequency of 40 kHz on a model compound, 1,2-^{13}C–^{15}N-glycine ethylester. The pulse sequence depicted in Fig. 1 was used to monitor the 1D heteronuclear transfer from N → Cα. The homonuclear transfer was also followed in a 1D experiment by selecting the Cα resonance and monitoring the build up on the C′ resonance. For the homonuclear case, the ^{1}H → ^{15}N CP was replaced by a ^{1}H → ^{13}C CP step, and after the CP step an additional filter was used to select only the Cα resonance. The filter consisted of a delay ($1/(4\Delta\nu_{iso})$) followed by a z-filter that ensured the C' resonance is dephased out in the X–Y place and only the Cα resonance is selected.

The plots in Fig. 3a, b show the homonuclear (Cα → C′) and heteronuclear (N → Cα) polarization-transfer profiles for 1,2-^{13}C–^{15}N-glycine ethylester for the RESORT and the het-RESORT experiment. Figure 3c shows a horizontal slice at a mixing time of 4 ms for the homonuclear RESORT (to be minimized) and the het-RESORT (to be maximized). Vertical traces through Fig. 3a, b, at 70 kHz rf field, are shown in Fig. 3d and represent the buildup of the RESORT and het-RESORT crosspeaks at the condition where the RESORT transfer is

minimized. The predicted effects are clearly seen. The corresponding experimental data for the PAR/PAIN sequences using cw irradiation on protons is given in Fig. 3e–h. The ^{13}C and ^{15}N rf amplitudes were set to 90 and 50 kHz respectively, during the resonant experiment while the ^{13}C and ^{15}N rf amplitudes were set to 50 kHz for the PAR/PAIN-CP experiment.

From Fig. 3a, b it is clearly evident that it is possible to separate the homonuclear and heteronuclear polarization transfer regimes for the amplitude-modulated sequences. At ν_{1H} of 60–70 kHz, the heteronuclear transfer is maximum, while the residual homonuclear transfer is minimum. Figure 3c shows that at a mixing time of 4 ms the homonuclear transfer is attenuated by about a factor of 6–8 in

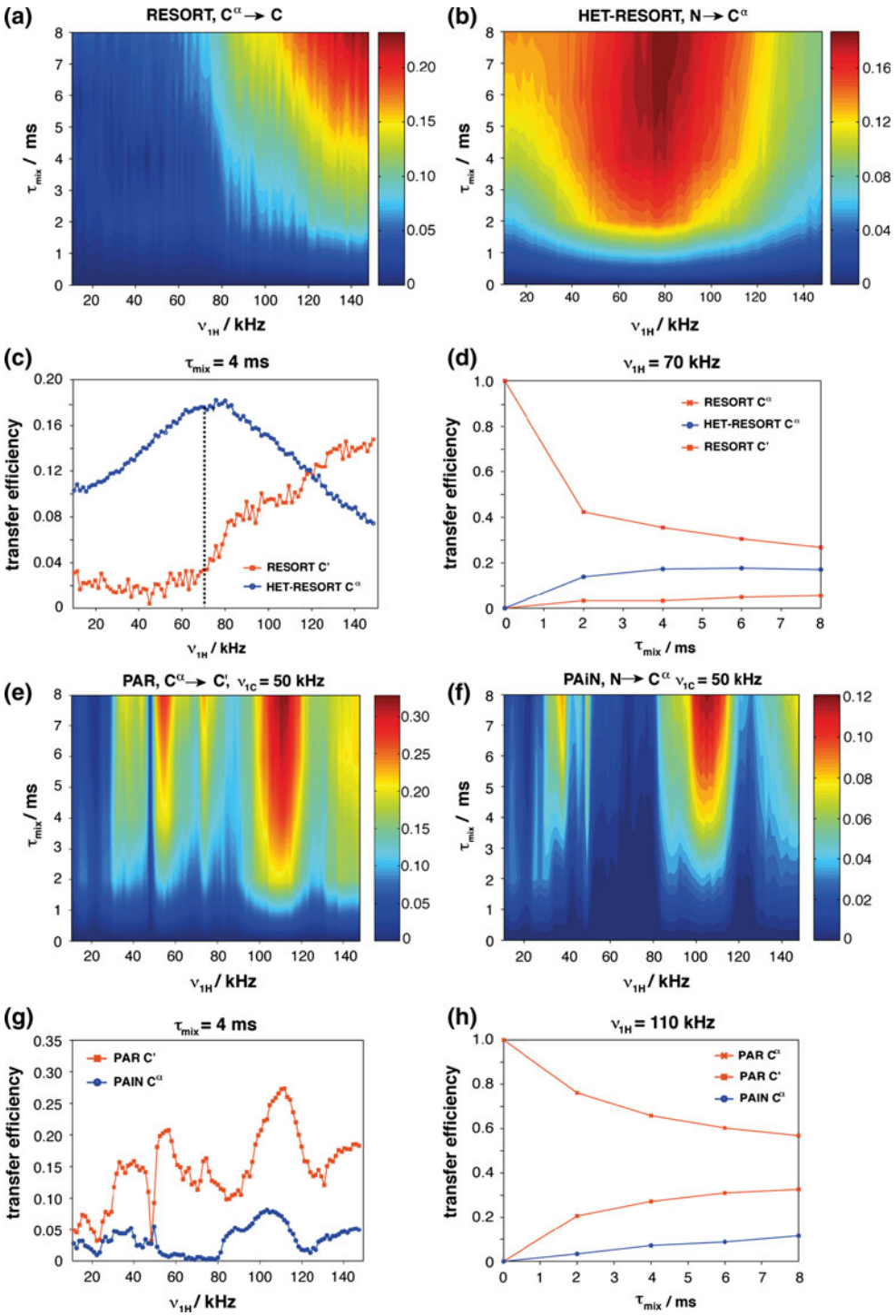

Fig. 3 Experimental polarization-transfer efficiencies from the Cα to C′ (*plots* **a**, **e**) and from the N to Cα (*plots* **b**, **f**) in 1,2-^{13}C-glycine ethyl ester as a function of the mixing time and the proton rf-field amplitude at a MAS frequency of 40 kHz. The ^{13}C and ^{15}N rf amplitudes were set to 90 and 50 kHz respectively for the amplitude modulated sequence while they were 50 kHz in case of the spin-lock sequences. In the remaining plots, slices for the efficiency of each polarization transfer are represented as a function of ^{1}H rf-field amplitude for a mixing time of 4 ms or as a function of the mixing time for a proton rf field amplitude of 70 and 110 kHz (maximum heteronuclear transfer in *plots* **c** and **g** for XiX decoupling and CW, respectively

comparison to the heteronuclear transfer, even though the resonance condition ($\omega_m = 2\omega_r$) for the homonuclear RESORT experiment is fulfilled. This experimental transfer profile of the RESORT and het-RESORT as a function of ν_{1H} closely resembles the one in the simulations (Fig. 2i). Figure 3d indicates that at the optimized condition, the build up of the homonuclear RESORT is slower than the heteronuclear transfer even though the cross-term between the two C–H dipolar couplings is bigger than the heteronuclear cross-term between the C–H and N–H dipolar couplings.

In contrast, the optimization of the continuous-wave second-order recoupling sequences as a function of ν_{1H} field shows that transfer profiles of the PAR and PAIN-CP condition are approximately similar (Fig. 3e–g). As expected from the magnitude of the second-order homonuclear and heteronuclear cross-terms, the buildup of the homonuclear transfer is much faster than the heteronuclear transfer (Fig. 3h).

Thus, as predicted from theory and simulation, it is indeed possible to separate the homonuclear and heteronuclear transfer condition in the recoupling sequences based on third-spin-mediated recoupling if phase-alternating sequences are used instead of cw irradiation. In general, the experimental results obtained on the model substance are consistent with the numerical simulations. Other resonance conditions were also investigated during the course of this research work; however the het-RESORT condition given by $\omega_m - \omega_r + \omega_{13C} - \omega_{15N} = 0$ gave so far the best results.

To demonstrate the applicability of the het-RESORT sequence, we measured two-dimensional ^{15}N–^{13}C correlation spectra of U-[^{13}C, ^{15}N] Ubiquitin at a MAS frequency of 40 kHz. Figure 4 shows an overlay of the 2D ^{15}N–^{13}C het-RESORT (red) and PAIN-CP (black) two-dimensional correlation spectra acquired with a mixing time of 4 ms. The het-RESORT was acquired at the resonance condition $\omega_m - \omega_r + \omega_{13C} - \omega_{15N} = 0$ while the PAIN-CP spectrum was acquired at the condition $\omega_{13C} = \omega_{15N}$. For the PAIN-CP experiment, the ^{1}H rf field was optimized to obtain maximum intensity, while for het-RESORT the proton rf field was set to approximately 60 kHz corresponding to minimum homonuclear transfer (see Fig. 3c) as demonstrated above through simulations and experiments on the model compound. No optimization of the ^{1}H amplitude was carried out for the het-RESORT experiment. Analogous to PAIN-CP, the most intense correlations appear in the N–Cα and N–CO regions of the 2D spectra. As predicted from theory and simulations, both sequences do not rely on direct N–C coupling for polarization transfer. However, for both the het-RESORT and PAIN-CP experiments, either first-order or second-order CP transfers can take place in uniformly labeled samples due to the presence of one-bond N–C and C–C dipolar couplings. The presence of direct N → C transfer pathways, which are usually neglected but can be significant, makes a direct quantitative comparison of the efficiency of the PAIN–CP and het-RESORT transfer difficult. We note that at best heteronuclear transfer conditions, both sequences have approximately the same performance, as can be seen in the extracted slices in Fig. 4b, c. An empirical comparison of the direct N–Cα and N–CO peak intensities in the het-RESORT and PAIN-CP spectra is provided in Fig. S3. We note that both spectra show essentially the same crosspeak intensities with increased sensitivity in the het-RESORT spectrum for Gly and Pro residues.

The main difference between the two spectra lies in the intensity of the side-chain atom resonances. At a mixing time of 4 ms, the het-RESORT spectrum (red, Fig. 4) has much less transfer out to the sidechains than the PAIN-CP spectrum (black, Fig. 4). While the significant sidechain intensity in the PAIN-CP experiment is easily explained by relayed processes, e.g. of the type N(CA)CX where CX denotes a sidechain carbon nucleus, which is fast due to the efficient PAR recoupling of the ^{13}C–^{13}C pathway, the peaks in the het-RESORT have two possible explanations (1) in an ideal experiment the transfer should be caused by direct N–C transfer either from the backbone or from sidechain nitrogen to the respective ^{13}C nuclei or (2) they could stem from relayed transfer which is not completely suppressed. A zoomed region of the het-RESORT spectrum of Fig. 4 is shown in Fig. 5 and the most important signals are assigned. Most observed peaks correspond to ^{15}N and ^{13}C nuclei with an internuclear distance of less than about 3.2 Å. For example intra-residue N–Cα and N–Cβ as well as N–Cγ correlations and sequential N^i–CO^{i-1}, N^i–$C\alpha^{i-1}$ correlations (see Fig. 5). A few peaks that correspond to medium-range correlations with distances up to about 4.5 Å are also visible (Fig. 5). Spectra at different mixing times are shown in the supporting information (Fig. S2).

Comparison of residual homonuclear transfer by PAR and RESORT

To estimate the degree of suppression of the homonuclear transfer in the PAIN/het-RESORT experiment we selectively observe the homonuclear relayed transfer step by replacing the ^{1}H → ^{15}N CP step in the pulse sequence of Fig. 1 by a ^{1}H → ^{13}C CP transfer step while leaving the mixing element and all experimental parameters of the het-RESORT and PAIN mixing element exactly identical to the one used in recording the heteronuclear correlation spectra. This essentially corresponds to recording a PAR/RESORT spectrum at the experimental conditions of the PAIN/het-RESORT. This modification leads to 2D

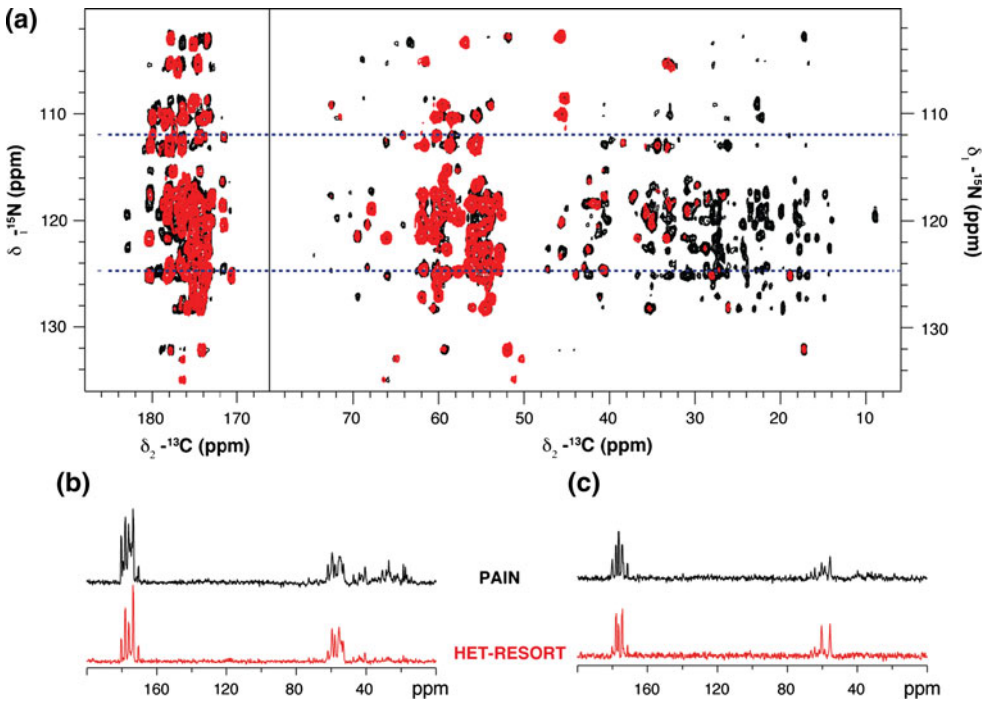

Fig. 4 **a** Two dimensional ^{15}N–^{13}C correlation experiment (*red* het-RESORT, *black* PAIN-CP) on a crystalline sample of U-[^{13}C, ^{15}N] Ubiquitin with the mixing time of 4 ms and MAS of 40 kHz. During the spin lock, the ^{13}C rf amplitude was set to 90 kHz (het-RESORT) and 50 kHz (PAIN-CP), the proton rf amplitude to 60 kHz (het-RESORT) and 83.1 kHz (PAIN-CP) and the ^{15}N rf amplitude was set to 50 kHz in both cases. The XiX modulation frequency ν_m was set to $\nu_m = 2\nu_r$. Two slices taken from the 2D spectra are represented in the figure corresponding to **b** 124.8 ppm; **c** 112.3 ppm. For both data sets, a total of 500 t_1 points with 32 scans each were acquired along the F1 dimension with a recycle delay of 3 s corresponding to a total acquisition time of 13.5 h

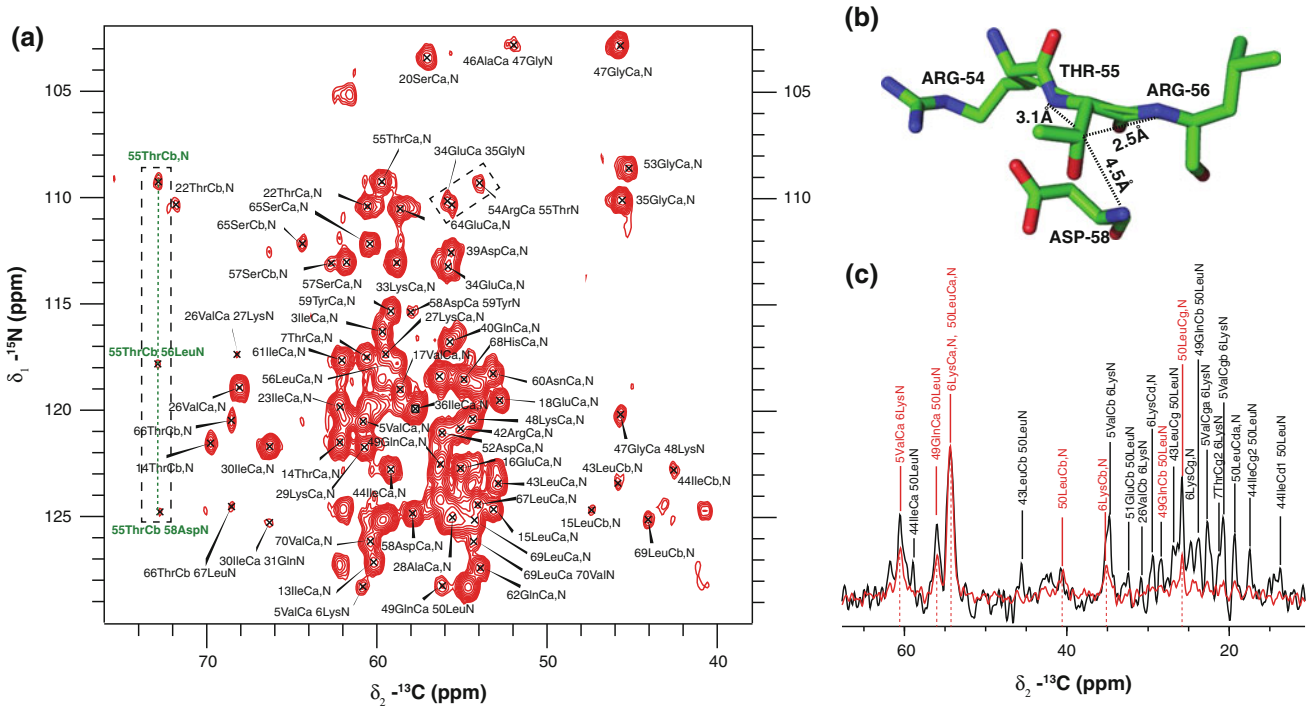

Fig. 5 **a** Zoomed region (N–Cα) from the 2D ^{15}N–^{13}C het-RESORT spectrum shown in Fig. 4. In most cases, the observed peaks are due to intra-residue or ^{i}N–$^{(i-1)}C\alpha$ correlations corresponding to the two shortest distances. Besides these, a few other correlations are also observable. For example, the *peaks* on the *green dotted line* include a medium-range correlation between Thr55Cb and Asn58N (shown by *dotted green line*). **b** Schematic representation of different residues from the Ubiquitin structure (PDB code: 1UBQ, Vijay-Kumar et al. 1987). The spatial distances between different nitrogen's and carbons are indicated with *dotted lines*. **c** Trace extracted at a nitrogen frequency of 128.2 ppm (6LysN and 50LeuN) resonances (*red*) compared with the corresponding frequency from the PAIN-CP spectrum (*black*). Strong peaks in the het-RESORT (with *red* label) correspond to short N–C distances (for the corresponding distances see Supplementary information) while most peaks that only appear in the PAIN-CP spectrum (*black* labels) correspond to longer N–C distances. These peaks can be assigned to relayed transfers

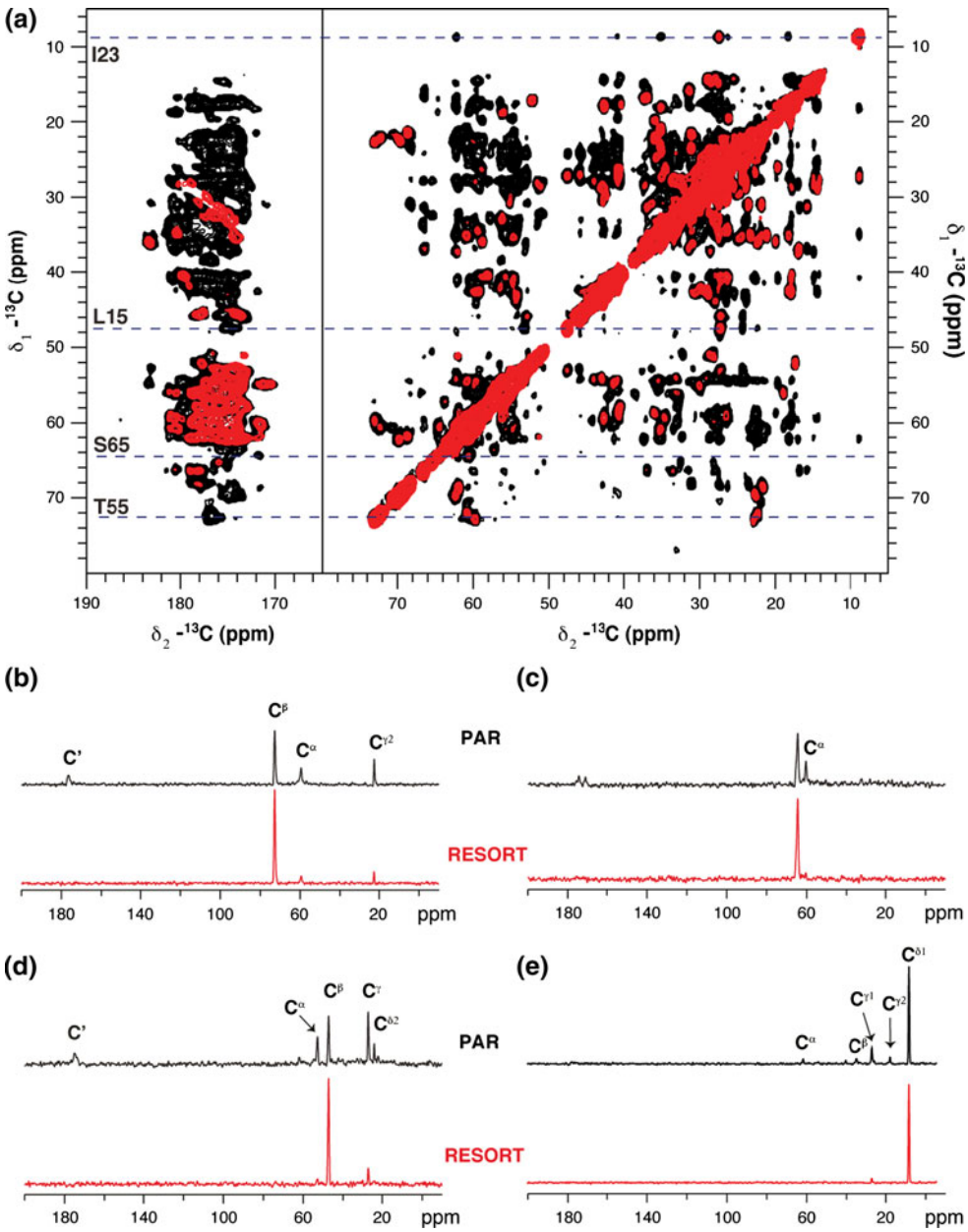

Fig. 6 **a** Two dimensional ^{13}C–^{13}C correlation spectra (*red* RESORT, *black* PAR) of a crystalline sample of U-[^{13}C, ^{15}N] Ubiquitin recorded with a mixing time of 4 ms and a MAS rate of 40 kHz. During the spin-lock, the ^{13}C rf amplitude was set to 90 kHz (for RESORT) and 50 kHz (PAR), the proton rf amplitude to 60 kHz (RESORT) and 83.5 kHz (PAR) and the ^{15}N rf amplitude was set to 50 kHz in both cases. The XiX modulation frequency ν_m was set to match the RESORT condition $\nu_m = 2\nu_r$. For both data sets, a total of 600 t_1 points with 16 scans each were acquired along the F1 dimension with a recycle delay of 3 s. The base contour level is set to 0.4 % of the maximum intensity in both the spectra. Several one dimensional (1D) slices taken from the 2D spectra (represented in Fig. 5) corresponding to **b** T55, 72.7 ppm; **c** S65, 64.4 ppm, **d** L15, 47.4 ppm and **e** I23 (8.3 ppm)

^{13}C–^{13}C homonuclear correlation spectra showing only the undesired homonuclear transfer during the PAIN/het-RESORT mixing elements. Figure 6 shows an overlay of the resulting ^{13}C–^{13}C 2D correlation spectra recorded using PAR and RESORT mixing with a mixing time of 4 ms. From the 2D plot, and in particular from the 1D traces b–e, it is clearly visible that the RESORT spectrum shows considerably less, and weaker, cross-peaks than the PAR spectra. Homonuclear correlations between side chain and carbonyl carbons are almost completely suppressed; correlations from Cα to side-chains and within the sidechain are significantly attenuated (by a factor of 3, typically). Most of the remaining peaks in the homonuclear RESORT spectra can be attributed to intra-residue correlations. They could not only result from the three-spin dipolar cross term but also from evolution of ^{13}C–^{13}C homonuclear one-bond scalar coupling during the spin-lock pulse or spin diffusion in the rotating frame.

Conclusions

We have introduced a heteronuclear resonant second-order recoupling experiment for the intermediate (about 20–50 kHz) MAS frequency range. We show that amplitude modulated sequences provide an efficient method to disentangle simultaneously occurring recoupling mechanism. In principle, there exist numerous conditions for

heteronuclear polarization transfer with or without the presence of sub-resonance conditions. Similar to the PAR and PAIN-CP experiments, the new sequence uses the third-spin assisted recoupling mechanism for polarization transfer and the effective Hamiltonian contains cross-term between two heteronuclear dipolar (N–H & C–H) couplings. In contrast to the PAIN-CP experiments, it is possible to experimentally separate, in good approximation, the homonuclear and heteronuclear polarization transfer pathways. This goal can be achieved at several resonance conditions, and here we discussed the $\omega_m - \omega_r + \omega_{1S} - \omega_{1M} = 0$ resonance condition in detail. The method was applied to U-[^{15}N, ^{13}C] labeled ubiquitin to record a 2D het-RESORT spectrum. At a mixing time of 4 ms most correlations observed can be attributed to a direct PAIN ^{15}N–^{13}C transfer without PAR relays.

Acknowledgments Financial support was provided by the Swiss National Science Foundation (Grant 200020_124611), the ETH Zurich and the CNRS (ANR-12-BS08-0013-01 XLproteinSSNMR). M.S. also acknowledges the Portuguese Foundation for Science and Technology for a post-doctoral grant—SFRH/BPD/65978/2009. We also acknowledge support from the European Commission under the Seventh Framework Programme (FP7), contract Bio-NMR 261863.

References

Bayro MJ, Huber M, Ramachandran R, Davenport TC, Meier BH, Ernst M, Griffin RG (2009) Dipolar truncation in magic-angle spinning NMR recoupling experiments. J Chem Phys 130:114506

Bennett A, Griffin R, Vega S (1994) Recoupling of homo- and heteronuclear dipolar interactions in rotating solids. NMR: Basic Princ Prog 33:1–77

Bennett A, Rienstra CM, Griffiths J, Zhen W, Lansbury P, Griffin R (1998) Homonuclear radio frequency-driven recoupling in rotating solids. J Chem Phys 108:9463–9479

Böckmann A, Gardiennet C, Verel R, Hunkeler A, Loquet A, Pintacuda G, Emsley L, Meier BH, Lesage A (2009) Characterization of different water pools in solid-state NMR protein samples. J Biomol NMR 45:319–327

Brinkmann A, Eden M, Levitt M (2000) Synchronous helical pulse sequences in magic-angle spinning nuclear magnetic resonance: double quantum recoupling of multiple-spin systems. J Chem Phys 112:8539–8554

Castellani F, van Rossum B, Diehl A, Schubert M, Rehbein K, Oschkinat H (2002) Structure of a protein determined by solid-state magic-angle-spinning NMR spectroscopy. Nature 420:98–102

Cavanagh J, Fairbrother W, Palmer A, Rance M, Skelton N (2007) Protein NMR spectroscopy. Principles and practice. Elsevier Academic Press, Amsterdam

de Paepe G (2012) Dipolar recoupling in magic angle spinning solid-state nuclear magnetic resonance. Annu Rev Phys Chem 63: 661–684

de Paepe G, Bayro M, Lewandowski J, Griffin R (2006) Broadband homonuclear correlation spectroscopy at high magnetic fields and MAS frequencies. J Am Chem Soc 128:1776–1777

de Paepe G, Lewandowski JR, Loquet A, Böckmann A, Griffin RG (2008) Proton assisted recoupling and protein structure determination. J Chem Phys 129:245101

de Paepe G, Lewandowski JR, Loquet A, Eddy M, Megy S, Böckmann A, Griffin RG (2011) Heteronuclear proton assisted recoupling. J Chem Phys 134:095101

Ernst RR, Bodenhausen G, Wokaun A (1989) Principles of nuclear magnetic resonance in one and two dimensional NMR. Oxford University Press, Oxford, UK

Ernst M, Geen H, Meier BH (2006) Amplitude-modulated decoupling in rotating solids: a bimodal Floquet approach. Solid State Nucl Magn Reson 29:2–21

Etzkorn M, Böckmann A, Lange A, Baldus M (2004) Probing molecular interfaces using 2D magic-angle-spinning NMR on protein mixtures with different uniform labeling. J Am Chem Soc 126:14746–14751

Grommek A, Meier BH, Ernst M (2006) Distance information from proton-driven spin diffusion under MAS. Chem Phys Lett 427: 404–409

Heise H, Luca S, de Groot B, Grubmuller H, Baldus M (2005) Probing conformational disorder in neurotensin by two-dimensional solid-state NMR and comparison to molecular dynamics simulations. Biophys J 89:2113–2120

Helmus JJ, Surewicz K, Apostol MI, Surewicz WK, Jaroniec CP (2011) Intermolecular alignment in Y145Stop human prion protein amyloid fibrils probed by solid-state NMR. Spectroscopy 133:13934–13937

Hohwy M, Jakobsen H, Eden M, Levitt M, Nielsen N (1998) Broadband dipolar recoupling in nuclear magnetic resonance of rotating solids: a compensated C7 pulse sequence. J Chem Phys 108:2686–2694

Hohwy M, Rienstra CM, Jaroniec C, Griffin R (1999) Fivefold symmetric homonuclear dipolar recoupling in rotating solids: application to double quantum spectroscopy. J Chem Phys 110: 7983–7992

Hohwy M, Rienstra CM, Griffin R (2002) Band-selective homonuclear dipolar recoupling in rotating solids. J Chem Phys 117: 4973–4987

Hong M, Jakes K (1999) Selective and extensive C-13 labeling of a membrane protein for solid-state NMR investigations. J Biomol NMR 14:71–74

Jaroniec CP, Tounge BA, Herzfeld J, Griffin RG (2001) Frequency selective heteronuclear dipolar recoupling in rotating solids: accurate (13)C-(15)N distance measurements in uniformly (13)C,(15)N-labeled peptides. 123:3507–3519

Kubo A, McDowell C (1988) Spectral spin diffusion in polycrystalline solids under magic-angle spinning. J Chem Soc Faraday Trans 84:3713–3730

Lamley JM, Lewandowski JR (2012) Simultaneous acquisition of homonuclear and heteronuclear long-distance contacts with time-shared third spin assisted recoupling. J Magn Reson 218:30–34

Lange A, Luca S, Baldus M (2002) Structural constraints from proton-mediated rare-spin correlation spectroscopy in rotating solids. J Am Chem Soc 124:9704–9705

Lange A, Seidel K, Verdier L, Luca S, Baldus M (2003) Analysis of proton-proton transfer dynamics in rotating solids and their use for 3D structure determination. J Am Chem Soc 125:12640–12648

Lange A, Scholz I, Manolikas T, Ernst M, Meier BH (2009) Low-power cross polarization in fast magic-angle spinning NMR experiments. Chem Phys Lett 468:100–105

LeMaster D, Kushlan D (1996) Dynamical mapping of *E. coli* thioredoxin via 13C NMR relaxation analysis. J Am Chem Soc 118:9255–9264

Leskes M, Madhu PK, Vega S (2010) Floquet theory in solid-state nuclear magnetic resonance. Prog Nucl Magn Reson Spectrosc 57:345–380

Lewandowski JR, de Paepe G, Griffin RG (2007) Proton assisted insensitive nuclei cross polarization. J Am Chem Soc 129: 728–729

Lewandowski JR, de Paepe G, Eddy MT, Struppe J, Maas W, Griffin RG (2009) Proton assisted recoupling at high spinning frequencies. J Phys Chem B 113:9062–9069

Loquet A, Bardiaux B, Gardiennet C, Blanchet C, Baldus M, Nilges M, Malliavin T, Böckmann A (2008) 3D Structure determination of the Crh protein from highly ambiguous solid-state NMR restraints. J Am Chem Soc 130:3579–3589

Loquet A, Lv G, Giller K, Becker S, Lange A (2011) 13C Spin dilution for simplified and complete solid-state NMR resonance assignment of insoluble biological assemblies. J Am Chem Soc 133:4722–4725

Manolikas T, Herrmann T, Meier BH (2008) Protein structure determination from 13C spin-diffusion solid-state NMR spectroscopy. J Am Chem Soc 130:3959–3966

Marulanda D, Tasayco ML, McDermott A, Cataldi M, Arriaran V, Polenova T (2004) Magic angle spinning solid-state NMR spectroscopy for structural studies of protein interfaces. Resonance assignments of differentially enriched *Escherichia coli* thioredoxin reassembled by fragment complementation. J Am Chem Soc 126:16608–16620

Meier BH, Earl W (1987) A double-quantum filter for rotating solids. J Am Chem Soc 109:7937

Morcombe CR, Gaponenko V, Byrd RA, Zilm KW (2004) Diluting abundant spins by isotope edited radio frequency field assisted diffusion. J Am Chem Soc 126:7196–7197

Nielsen AB, Székely K, Gath J, Ernst M, Nielsen NC, Meier BH (2012) Simultaneous acquisition of PAR and PAIN spectra. J Biomol NMR 52:1–6

Samoson A, Tuherm T, Past J (2001) Ramped-speed cross polarization MAS NMR. J Magn Reson 149:264–267

Scholz I (2010) Operator based Floquet theory and it's applications to solid-state NMR. Diss ETH, pp 1–200

Scholz I, Meier BH, Ernst M (2007) Operator-based triple-mode Floquet theory in solid-state NMR. J Chem Phys 127:204504–204513

Scholz I, Huber M, Manolikas T, Meier BH, Ernst M (2008) MIRROR recoupling and its application to spin diffusion under fast magic-angle spinning. Chem Phys Lett 460:278–283

Scholz I, Meier BH, Ernst M (2010a) NMR polarization transfer by second-order resonant recoupling: RESORT. Chem Phys Lett 485:335–342

Scholz I, van Beek JD, Ernst M (2010b) Operator-based Floquet theory in solid-state NMR. Solid State Nucl Magn Reson 37:39–59

Schubert M, Manolikas T, Rogowski M, Meier BH (2006) Solid-state NMR spectroscopy of 10% 13C labeled ubiquitin: spectral simplification and stereospecific assignment of isopropyl groups. J Biomol NMR 35:167–173

Seuring C, Greenwald J, Wasmer C, Wepf R, Saupe SJ, Meier BH, Riek R (2012) The mechanism of toxicity in HET-S/HET-s prion incompatibility. PLoS Biol 10:e1001451

Smith S, Levante T, Meier BH, Ernst R (1994) Computer simulations in magnetic resonance: an object oriented programming approach. J Magn Reson Ser A 106:75–105

Stevens TJ, Fogh RH, Boucher W, Higman VA, Eisenmenger F, Bardiaux B, van Rossum B-J, Oschkinat H, Laue ED (2011) A software framework for analysing solid-state MAS NMR data. J Biomol NMR 51:437–447

Suter D, Ernst R (1985) Spin diffusion in resolved solid-state NMR spectra. Phys Rev B 32:5608–5627

Szeverenyi N, Sullivan M, Maciel G (1982) Observation of spin exchange by two-dimensional fourier transform 13C cross polarization-magic-angle spinning. J Magn Reson 47:462–475

Takegoshi K, Nakamura S, Terao T (2001) C-13–H-1 dipolar-assisted rotational resonance in magic-angle spinning NMR. Chem Phys Lett 344:631–637

Takegoshi K, Nakamura S, Terao T (2003) 13C–1H dipolar-driven 13C–13C recoupling without 13C rf irradiation in nuclear magnetic resonance of rotating solids. J Chem Phys 118: 2325–2341

Tycko R, Dabbagh G (1990) Measurement of nuclear magnetic dipole-dipole couplings in magic. Chem Phys Lett 173:461

van Melckebeke H, Wasmer C, Lange A, Ab E, Loquet A, Böckmann A, Meier BH (2010) Atomic-resolution three-dimensional structure of HET-s(218–289) amyloid fibrils by solid-state NMR spectroscopy. J Am Chem Soc 132:13765–13775

Verel R, Baldus M, Nijman M, Vanos J, Meier BH (1997) Adiabatic homonuclear polarization transfer in magic-angle-spinning solid-state NMR. Chem Phys Lett 280:31–39

Verel R, Ernst M, Meier BH (2001) Adiabatic dipolar recoupling in solid-state NMR: the DREAM scheme. J Magn Reson 150: 81–99

Verhoeven A, Williamson P, Zimmermann H, Ernst M, Meier BH (2004) Rotational-resonance distance measurements in multi-spin systems. J Magn Reson 168:314–326

Vijay-Kumar S, Bugg C, Wilkinson K, Vierstra R, Hatfield P, Cook W (1987) Comparison of the three-dimensional structures of human, yeast, and oat ubiquitin. J Biol Chem 262:6396–6399

Vranken W, Boucher W, Stevens T, Fogh R, Pajon A, Llinas P, Ulrich E, Markley J, Ionides J, Laue E (2005) The CCPN data model for NMR spectroscopy: development of a software pipeline. Proteins 59:687–696

Wasmer C, Lange A, van Melckebeke H, Siemer AB, Riek R, Meier BH (2008) Amyloid fibrils of the HET-s(218–289) prion form a beta solenoid with a triangular hydrophobic core. Science 319:1523–1526

Williamson P, Verhoeven A, Ernst M, Meier BH (2003) Determination of internuclear distances in uniformly labeled molecules by rotational-resonance solid-state NMR. J Am Chem Soc 125: 2718–2722

Zech S, Wand A, McDermott A (2005) Protein structure determination by high-resolution solid-state NMR spectroscopy: application to microcrystalline ubiquitin. J Am Chem Soc 127:8618–8626

Zhou DH, Shea JJ, Nieuwkoop AJ, Franks WT, Wylie BJ, Mullen C, Sandoz D, Rienstra CM (2007) Solid-state protein-structure determination with proton-detected triple-resonance 3D magic-angle-spinning NMR spectroscopy. Angew Chem Int Ed 46: 8380–8383